INTERFEROMETRIC METHODS FOR ALIGNING AND MEASURING TEST SURFACES

Emily Heaton

A Master's Report Submitted to the Faculty of the

COLLEGE OF OPTICAL SCIENCES

In Partial Fulfillment of the Requirements

For the Degree of

MASTER OF SCIENCE

In the Graduate College

THE UNIVERSITY OF ARIZONA

2016

Abstract:

Wavefront interference permits for a variety of tests that determine the optical quality of a mirror. Newton and Fizeau interferometers, as well as the basics of fringe and aberration analysis, were discussed to gain a fundamental understanding of interference patterns and how to map them to surface figure. The null testing configurations – retro-reflection as well as front- and back-focus – for flat and spherical surfaces were interferometrically tested to help characterize a lens of unknown parameters. As a result the index of refraction ($n = 1.499 \pm 0.005$) was calculated for a plano-convex lens using values found for the thickness of the lens ($t = 1.012 \pm 0.0014\ inches$) and the distance between the back- and front-focus null-configurations ($s = 0.678 \pm 0.001\ inches$). Additionally, the radius of curvature was determined interferometrically ($r_{int} = 2.953 \pm 0.001\ inches$), and compared to the radius of curvature found using a spherometer ($r_{sph} = 2.90 \pm 0.005\ inches$). The resulting nominal percent-difference between the two calculated radii is 1.7%. The rough alignment of an off-axis parabola (OAP) was also performed, such that the sagittal and tangential astigmatic lines were minimized – this is an important step as astigmatism dominates the alignment of an OAP.

Table of Contents

Table of Figures

1 Introduction

Interferometric testing is one of the most powerful optical testing tools, the use of which spans research fields and industries. From the measurement of gravitational waves, to aligning the optical components of guidance units, to configuring optical surfaces, it is interferometric testing that creates a practical means to do so.

The focus of this report is to gain optical testing experience with interferometers. A discussion of Newton and Fizeau interferometers is developed to understand the physical phenomena of constructive and destructive interference. This knowledge can be combined with aberration theory to determine the aberrations present in the optic: spherical, coma, astigmatism, and higher order terms. A good understanding of these theories allows optics shops to make quick adjustments when polishing lenses and mirrors, and is discussed in the context of OPTI 597A, Optical Shop Practices.

Several null configurations were aligned for a flat and plano-convex lens, including a front- and rear-focus and retro-reflection. The locations of the lens for each configuration is important for determining lens parameters, such as radius of curvature and index of refraction.

Finally, this paper will discuss the rough alignment of an off-axis parabola (OAP). The fabrication, testing, and use of OAP's are becoming more mainstream, thus this was going to be a focus of the report. However, due to limitations in the degrees of freedom a fine alignment could not performed. After observing and minimizing the astigmatic lines indicative of a rough alignment, it was decided to begin focusing on the plano-convex null configurations.

These exercises provided experience with alignment and the use of a commercial interferometer (Wyko 6000 Phase Shifting Fizeau). This experience was the primary goal for preparing for a future in optical testing.

2 Interferometric testing

2.1 Newton Interferometer

One of the most basic designs for an interferometer is the Newton Interferometer. It often involves placing a lens onto a well-measured reference surface with the desired surface figure, and observing light reflecting off of the surfaces of each piece. This will generate fringes corresponding to some small air gap between each optic. While this method is not the most advanced for in-depth measurements of an optic's surface metrics, it is the simplest method for determining an overall surface figure and its relatively larger variations from optimal.

This method was originally preferred in optics shops as it gave a quick idea to the polishers of how close their optic was to being finished. By observing different patterns in the fringes, polishers could easily determine high and low spots, or an optic's radius of curvature. With a Newton interferometer setup, a polisher could make several passes on their lens, put it back on the reference, observe the fringes for any irregular spots, and repeat until their lens met requirements.

A Newton interferometer consists of two surfaces nearly in contact and illuminated by a light source. This interferometer is most commonly used when fabricating flat or spherical transmissive optics. A flat optic or a spherical optic with a *large* radius of curvature is compared to a reference flat of known surface figure,

while a spherical optic of *smaller* radius is laid on a reference optic that has the desired radius of curvature for the unit under test (UUT) (see Figure 1).

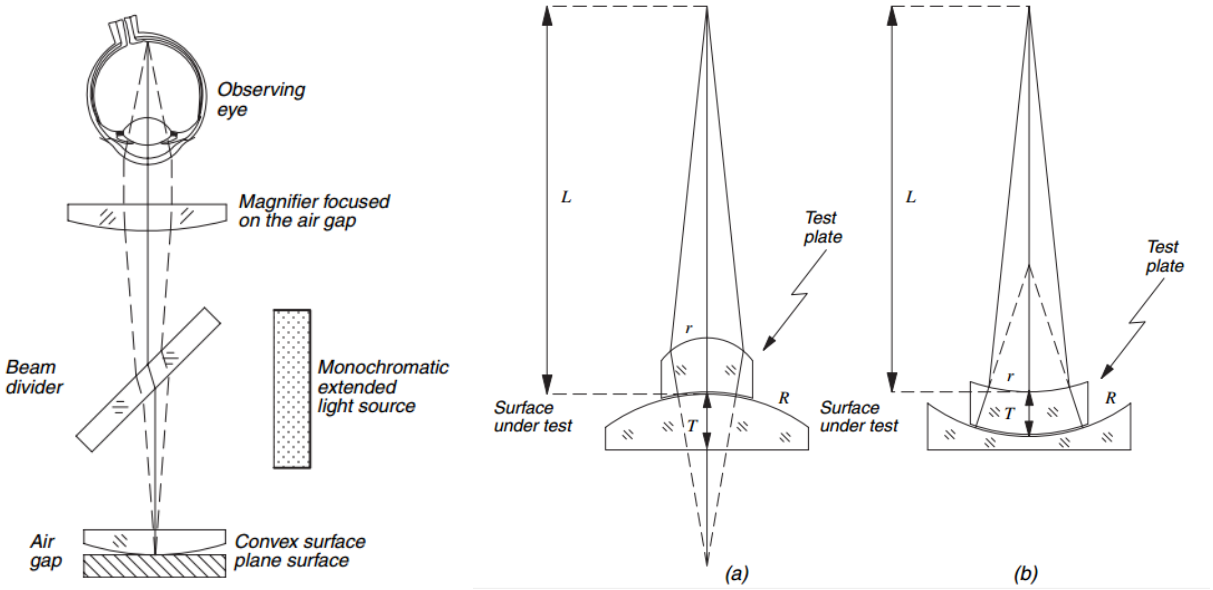

Figure 1: Newton Interferometer using a flat reference (left). Newton Interferometer for a spherical reference (right); convex surface (a), and concave surface (b). (Malacara, 2007)

Note that a Newton interferometer is best used when the air gap between the UUT and the reference surface is no more than a few wavelengths thick. While this test can be used to determine a quantitative value of the surface figure of a UUT, it is often used to help determine the overall nonuniformity of the air gap thickness by observing and interpreting Newton's fringes. An example of Newton's fringes for this test are shown below in the figure below:

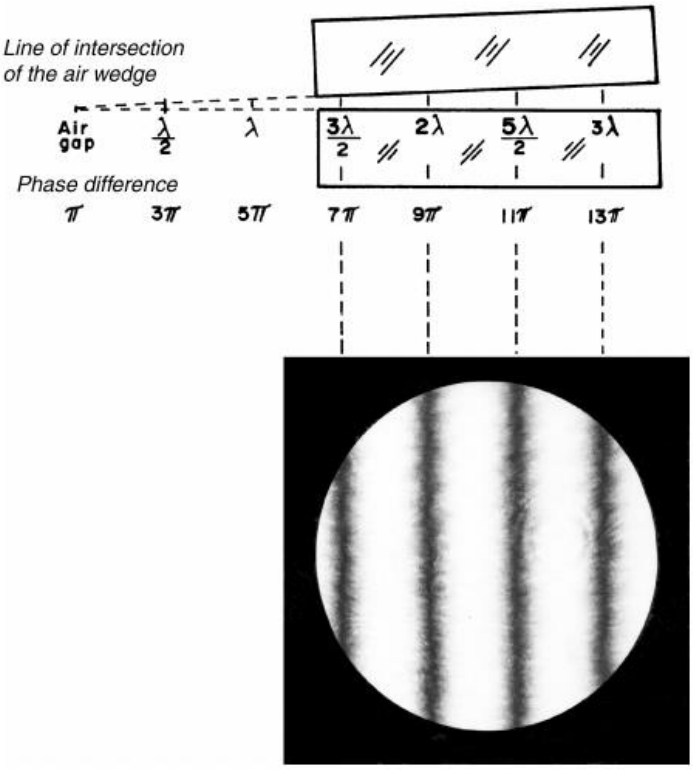

Figure 2: Example of Newton's fringes for two perfect optical flats separated by a wedge-shaped air gap. (Malacara, 2007)

In the figure above, two perfect optical plates are put in close proximity with a wedge-shaped air gap between them. For this section, we will focus on the case of using a reference flat to derive the logic behind a Newton Interferometer. In practice the plates will generally not be able to touch at their corners, so a virtual contact point is projected as shown in the figure. Monochromatic light of wavelength λ is normally incident on the system (compared to the reference flat), and reflects off both the bottom side of the UUT and the top of the reference flat. As the horizontal distance along the system increases by x, the vertical distance between the plates increases by αx, where α is the wedge slope (or angle, for small angle approximations) between the plates. Thus, the optical path difference (OPD) of the light reflecting off of the reference flat is $2\alpha x$. Finally, we must account for the phase shift of π that occurs upon reflection between a lower-index medium to a higher-index medium – this phase shift can be accounted for by adding $\lambda/2$ to the OPD. The final OPD is shown below in equation 1 (Murty, 1978):

$$OPD = 2\alpha x + \frac{\lambda}{2} \quad (1)$$

This equates to a phase shift of ϕ (Murty, 1978):

$$\phi = \frac{2\pi}{\lambda} OPD = \frac{2\pi}{\lambda}(2\alpha x) + \pi \quad (2)$$

For the case of a coherent source, the Intensity pattern (and thus interference) between the light reflected from the lower surface of the UUT and the upper surface of the reference flat can be modeled as follows:

$$I = \left| E_{UUT} + E_{ref} \cos\phi \right|^2 \quad (3)$$

Where E_{UUT} is the electric field amplitude of the light reflecting off of the surface of interest, E_{ref} is the electric field amplitude of the light reflecting off of the reference surface, and ϕ is the phase difference between the two, as shown in Equation 2.

Combining this model with the phase shift defined in equation 2 yields the cases for bright and dark fringes based on the round-trip distance between the surfaces (Murty, 1978):

$$Bright\ Fringes: \qquad 2\alpha x = \frac{(2n-1)\lambda}{2}$$
$$Dark\ Fringes: \qquad 2\alpha x = n\lambda$$

Additionally, the distance, d, between adjacent bright or dark fringes is determined by the definition of the slope α and wavelength of monochromatic light used for the test (Murty, 1978).

$$d = \Delta x_{fringes} = \frac{\lambda}{2\alpha} \quad (4)$$

Many of the principles derived above for flat-on-flat interferometric testing also apply to the case of a spherical optic on a reference flat. This second case is more commonly used as it is unlikely a UUT will be perfectly flat to begin with. In the case of a spherical UUT, there will be a central bright fringe where the optics contact, and a series of circular fringes whose radii are determined by the radius of curvature of the optic as shown in equation 5 and Figure 3. If the UUT is indeed intended to be a flat, the observation of circular fringes is a quick way to confirm more polishing is needed (Murty, 1978).

$$r_n = \sqrt{nR\lambda} \quad (5)$$

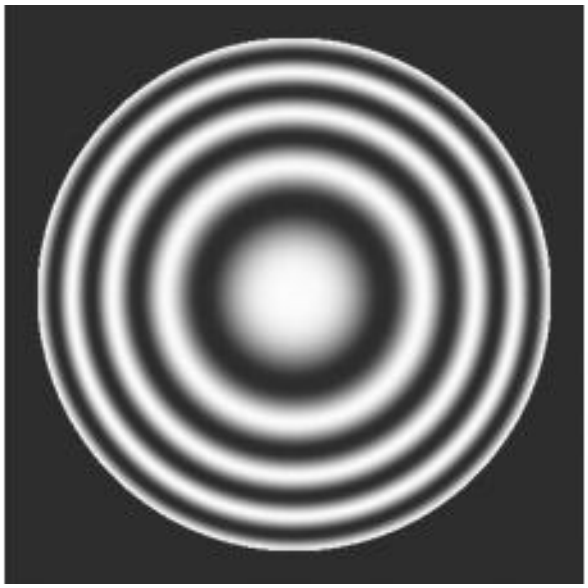

Figure 3: Circular fringes from a spherical UUT on a reference flat. (Malacara, 2007)

By being able to form a relationship between the distance between fringes and the radius of curvature or tilt of a lens (such as those in equations 4 or 5), optical polishers are able to make quick measurements on an output screen and instantly relate it to errors in their lens. This method does not need to be highly accurate due to its ease of repeatability.

While the Newton Interferometer is a simple method for optical testing, it has the drawback that the airgap can only be several wavelengths wide. This has another consequence that the surfaces must be thoroughly cleaned to ensure there is no dust on either surface, as this dust has the potential to be larger than the air gap.

2.2 Fizeau Interferometer

A Fizeau interferometer is similar in principle to the Newton interferometer, with the most notable difference being a larger air gap between the UUT and the reference. Due to this larger distance, Fizeau interferometers require extra care when aligning the optical surfaces, but less care when cleaning the optics. Companies such as Wyko and Zygo have made user-friendly interferometers that are mostly pre-aligned, and only require some adjustments of the reference surface and the UUT to the reference. Nowadays, most companies dealing in optics will have these pre-packaged interferometers so their technicians can use them nearly as easily as the Newton setup to determine surface figure and test requirements.

2.2.1 Illumination Source and basic design for Fizeau Interferometers

Fizeau interferometers are preferred when the air gap between the UUT and the reference surface needs to be greater than a few wavelengths. However, Fizeau interferometers are much more sensitive to the angle of incoming light, as derived below. Thus a Fizeau interferometer has a light source consisting of a pinhole and a collimating lens.

For two reflective surfaces and incoming light at an incident angle θ, we have the following setup in the figure below:

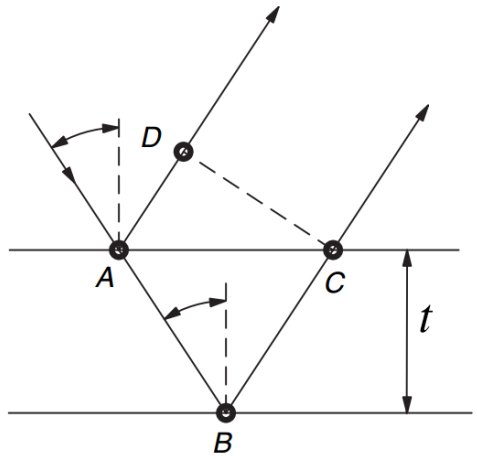

Figure 4: Ray Diagram for Calculation of OPD between two reflected rays from an air gap of thickness t and angle of incidence ϑ. (Malacara, 2007)

From figure 3 above, the OPD can be determined as (Murty, 1978):

$$OPD = AB + BC - AD = 2t\cos\theta \tag{6}$$

For small angles, the OPD can be rewritten as follows (Murty, 1978):

$$OPD = 2t\cos\theta \approx 2t - t\theta^2 \tag{7}$$

Since the point of interferometry is to determine the variations in the air gap between the UUT and the reference surface (and thus the surface figure of the UUT), we are primarily interested in the first term of equation 7. Since the thickness t is much larger for a Fizeau interferometer than for a Newton interferometer, the incident angle θ must be much smaller to cause the second term of equation 7 to drop off. Because of this, it is often best practice to use a pinhole light-source with a collimating lens for the Fizeau interferometer (figure 4 below):

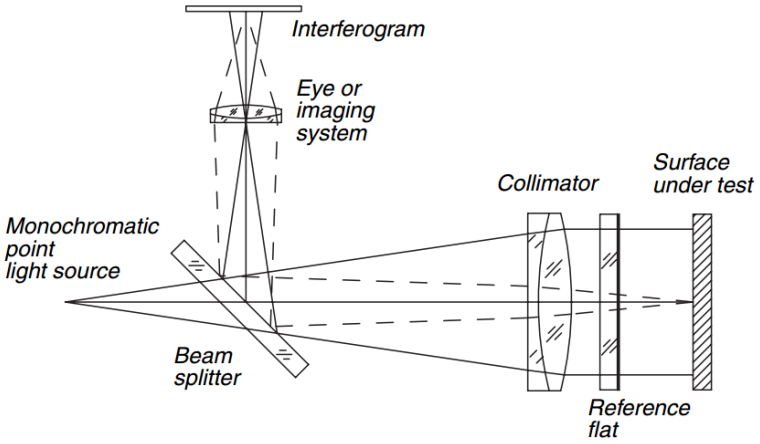

Figure 5: Basic Design of a Fizeau Interferometer. (Malacara, 2007)

The figure above is a basic design for a Fizeau interferometer. Various components of the design can be changed to modernize or improve the setup. This includes replacing the output screen with a CCD to digitally record the data, or placing the reference surface on a flexure that can be shifted by fractions of a wavelength via a piezoelectric transducer (PZT) to reduce the noise in the system and boost accuracy. This is known as a phase shifting interferometer.

2.2.2 Phase shifting

Theoretically, a static interferometer can be used to measure an optical surface to the limit of the resolution and magnification of the system. However, in reality we run into issues: noise in the photodetectors, needing the exact center of fringes for accurate measurements, and data only being reliably collected along the fringe centers. Phase shifting addresses these issues, as the method does not rely on locating fringe-centers. Secondly, measurements can be taken at every pixel of a photodetector, greatly increasing the data gathered from an interferogram.

In OPTI 524, Optical Systems Engineering, my team used the Hariharan 5-step phase-shifting algorithm for our phase shifting Fizeau Interferometer (Hariharan, 1999). This method required taking an image of the interferogram at intervals of $\lambda/4$ as the reference surface shifts from 0 to λ. Then, each pixel's final phase difference – and thus OPD and surface figure – is calculated using the intensity values measured at that pixel for each shift of the reference surface. We chose this relatively simple algorithm due to the limitations of the equipment we had on hand, as more shifts require either smaller, more accurate PZT's or a larger stack of them for a larger range of motion. An image of our interferometer is below:

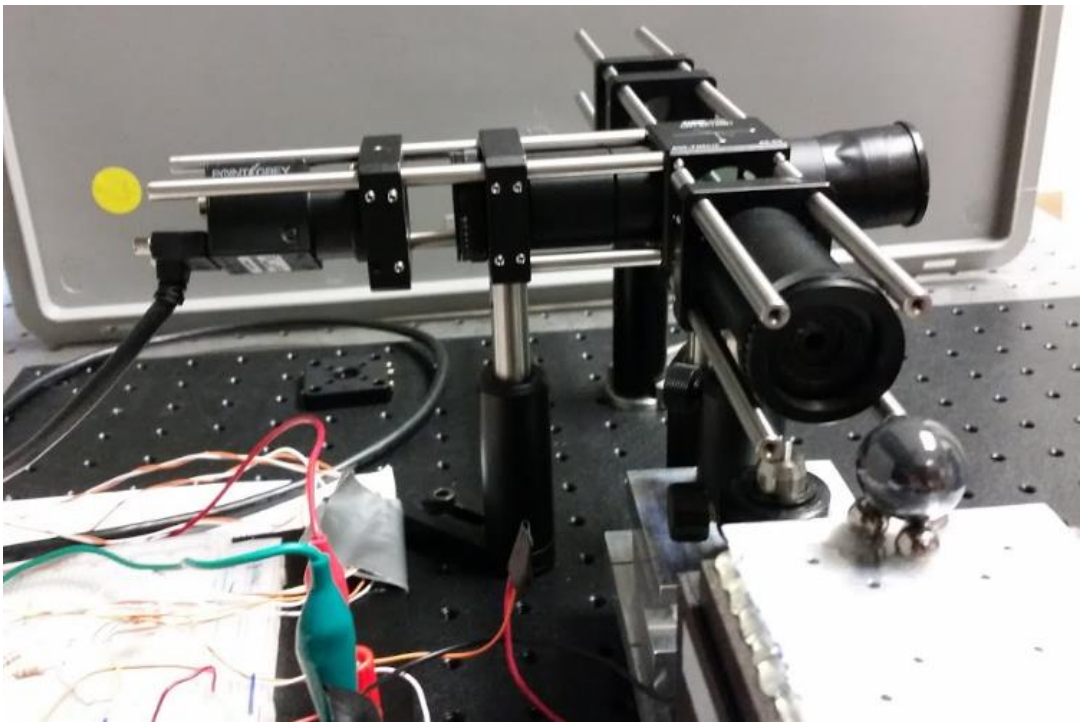

Figure 6: OPTI 524 Fizeau Phase Shifting Interferometer with Silicon-Nitride Ball UUT.

A good way to improve the results of phase shifting is to increase the number of shifted interferograms used to calculate the final phase difference of wavefronts reflecting off the UUT and the reference. A number of papers discuss algorithms with more than the 5-step Hariharan method. It is interesting to note that the algorithms are much easier to derive than it is to match the required technology – there is a 1997 Zygo paper outlining "an attempt to look far into the future" with a 101-step phase shifting algorithm (DeGroot, Peter, 1997).

As seen in OPTI 524, a phase shifting Fizeau Interferometer can be made from scratch by students for a few hundred dollars, some borrowed parts, and a couple months of work. But realistically an optics shop will be purchasing a pre-packaged unit from a company like Zygo or Wyko due to the ease of use as the software behind running the interferometers is very intensive.

2.3 Interpreting Interferograms

In section 2.1, I discussed the basic concept of fringe patterns due to a variation in air gap between a UUT and a reference. This is shown for the case when the two optics are tilted relative to each other (Figure 2). In reality there are a whole myriad of aberrations that a polisher must know how to translate in order to figure out the shape of a surface. The lower order aberrations – such as tilt and defocus – can be considered effects of misalignment of the optical system. Higher order aberrations – such as coma, spherical aberration, and astigmatism – can be considered effects of the UUT's surface condition. All of these aberrations can be indefinitely taken to higher and higher orders (such as secondary coma or secondary astigmatism) to form a series solution to an optical surface's error (Schwiegerling, 2014). However, many times in practice we don't concern ourselves with the order of an aberration (whether it is astigmatism or secondary astigmatism) – the primary takeaway from an interferogram is the type of basic aberration listed above since this gives us the shape of a surface.

An interferogram of a single aberration is relatively easy to translate into surface figure errors using our understanding of phase differences and destructive interference (equation 3), and a modelling of the wavefront errors for each aberration. This is shown in Figure 7 below, where the x and y axes are positional coordinates, and the z-axis is the wavefront error.

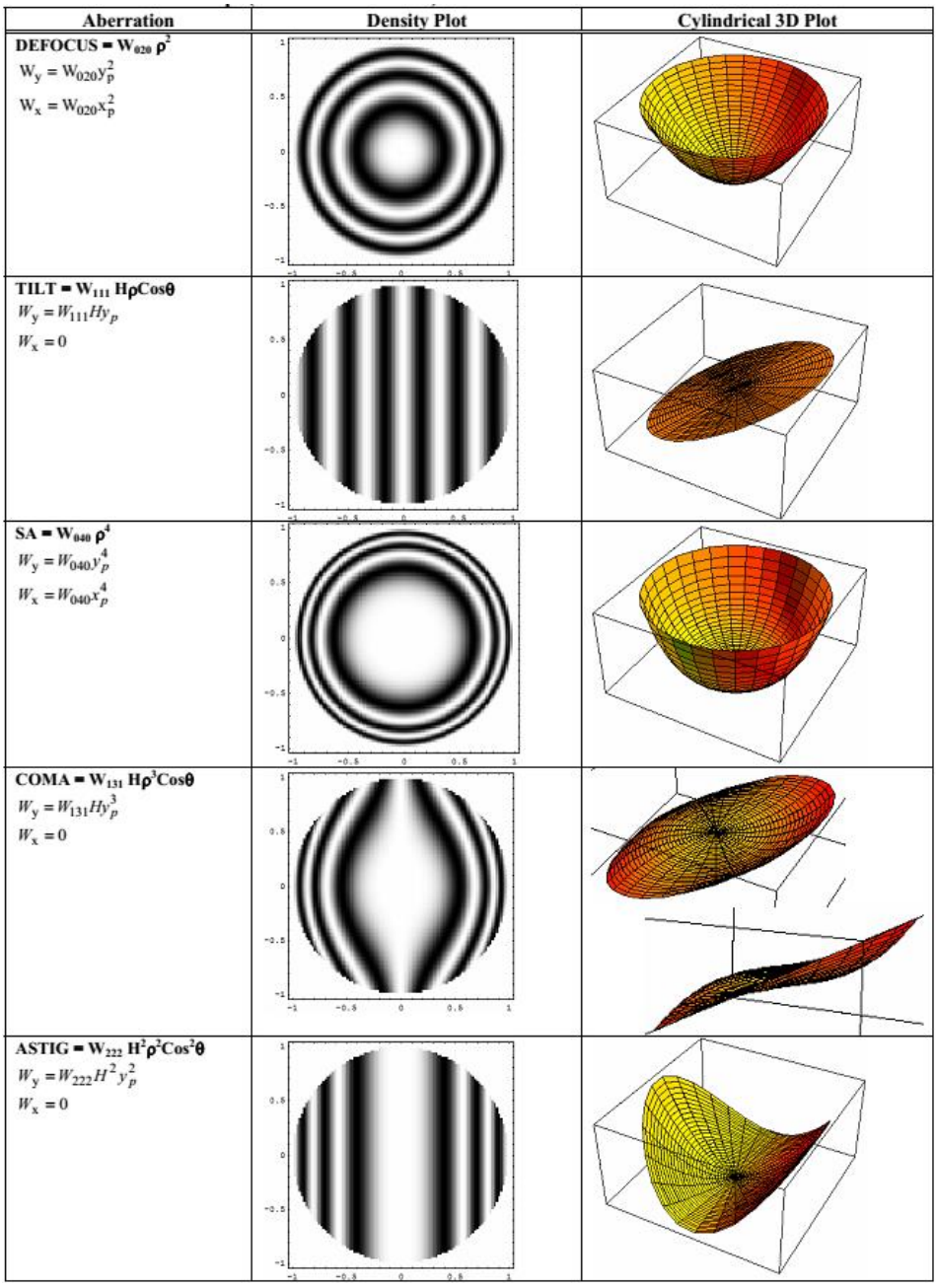

Figure 7: Aberration examples with example interferograms and wavefront errors (Green, n.d.)

During fabrication, deciphering the interferogram is vital as it gives a quick answer of how to continue polishing the optic. This was a frequent step in OPTI 597A, Optical Shop Practices, when fabricating and polishing the mirrors for a Dahl-Kirkham telescope. To introduce the desired conic constant for the mirror, large W-shaped strokes were used to polish down the interior of the mirror, while leaving the edges

relatively high. This effectively made a "hole" which was later spread out. As expected, my mirror's interferograms were indicative of spherical aberration when tilt was added to the system in the form of tilt fringes with rounded edges.

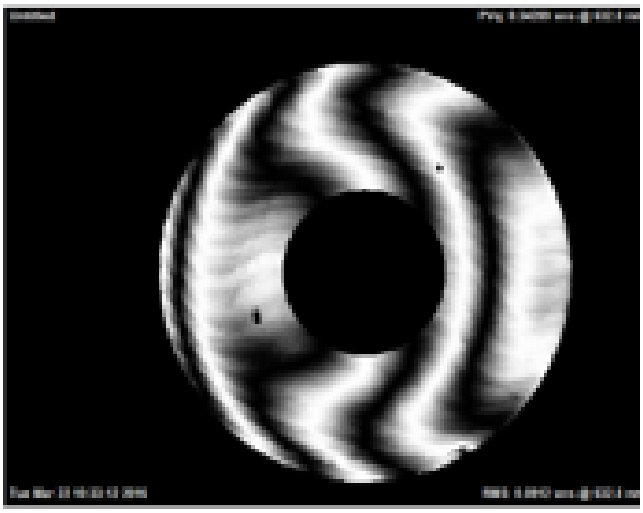

Figure 8: Interferogram from OPTI 597B, Primary Mirror with Spherical Aberration

From this interferogram it could be determined that the "hole" needed to be spread by doing smaller W-shaped patterns. This mirror had easily readable interferograms as it did not have many aberrations contributing to its surface figure, and adding the effects of tilt to an aberration is simple. Through multiple iterations of polishing and testing, the mirror was finalized. The final interferogram of the mirror with a null corrector test is shown in Figure 9 below.

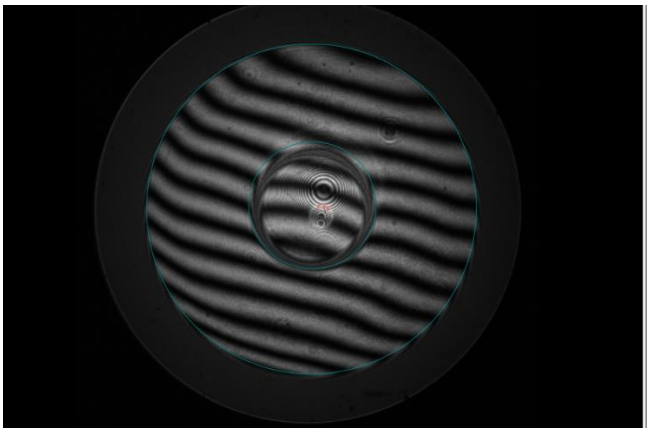

Figure 9: Final Interferogram of OPTI 597B Primary Mirror

Since this mirror is elliptical, and not spherical, a null corrector test was done to determine if the mirror was finished configuring. By placing a correcting lens between the reference surface and the primary mirror, the correcting lens can introduce an opposite amount of spherical aberration to that of the primary mirror such that the fringes on the interferogram are straight. To know if the configuration on the primary is finished, the placement of the corrector lens must correspond to the desired conic constant of the primary to form straight fringes. Using Zemax, it was found that the distance from element focus to null

corrector focus must be ideally centered around 15.59mm. Since the fringes were straight (to less than a quarter-wave error), it was determined that this primary was done configuring.

The mostly straight tilt fringes of the above interferogram demonstrate that most of the aberrations in the optical surface were successfully removed. Polishing this mirror was fairly straightforward due to having mostly spherical aberrations while a classmate had a harder time since another mirror that had both spherical aberration and astigmatism.

Things can quickly become more complicated when we begin combining higher order aberrations by adding the different order wavefront errors with varying weights. An example of this is shown below, where the figures have varying levels of coma, spherical aberration, and astigmatism.

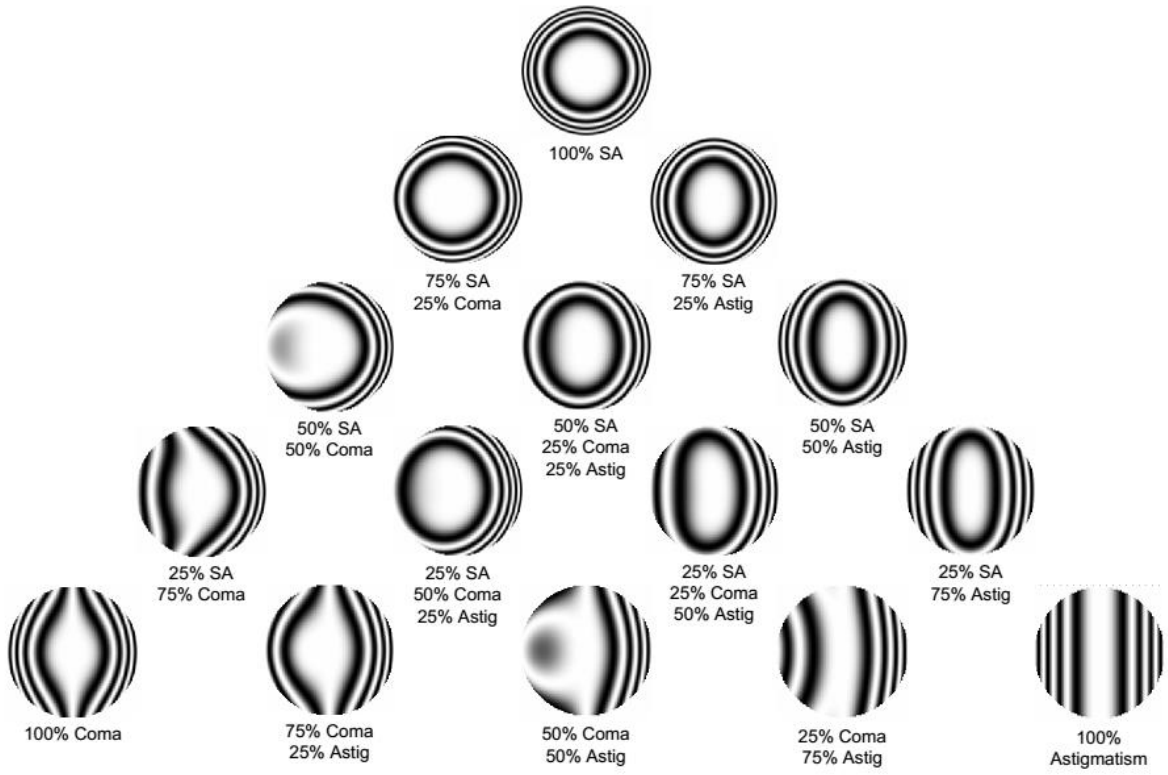

Figure 10: Interferograms with varying levels of Spherical Aberration, Coma, and Astigmatism (Green, n.d.)

Even in the figure above, someone with minor experience could determine the different types of aberration. However, during fabrication an expert with years of experience is often needed to pass this initial hurdle when an optic has complicated interferograms like that shown in Figure 15.

3 Null testing configurations

A null test is when the interferometer and the UUT are aligned such that the interference pattern on the output screen is uniform – no fringes (i.e. a null fringe) are observed. Null test configurations for spherical or conic surfaces may be used during interferometric testing to determine the radius of curvature, or for flat surfaces to observe surface figure. For a spherical surface we can see the effects that shifting the optic has on the null fringe, while for a flat surface any fringes visible are an apparent sign of deviations

from a perfect flat (subtracting the tilt that is often injected into the system). Note that for a flat surface, any shifting is not necessary and is in essence the original test described in section 2.2.1.

In the case of this report, a Wyko 6000 Fizeau phase shifting interferometer was used. This will be discussed further in sections 3.2 and 3.3 where the various null-test configurations for a flat and plano-convex surfaces are found. In order to generate a null configuration, the goal is to not introduce any aberrations into the system – the light coming from the Wyko is the light heading back into the Wyko (barring an inversion or uniform interference). For a perfect null-configuration there are no fringes, but some tilt was injected into the system in order to better translate the interferograms using the knowledge from the previous section.

3.1 Characterization of Lenses for Null Testing

Before a description of the null testing is given, a characterization of the lens tested is first provided for the metrics that are not determined inteferometrically. The other metrics are discussed in the next section, where the null configurations were used with an interferometer. The lens that will hereby be referred to as lens 1 was completely uncharacterized, and no information about it was known. Therefore, all characteristics had to be measured and/or calculated. A caliper, micrometer, and spherometer were used for the measurements of this lens.

3.1.1 Finding the Diameter of the lens using a Caliper

With a caliper, the diameter of lens 1 was measured to be 4.316 ± 0.001 inches. To measure the diameter, the calipers were spread to approximately the widest location, and translated back and forth along the outer edge to determine the widest length. The lens was then rotated a few times to confirm the diameter since there were some large chips in the glass. The uncertainty on the caliper reading is the smallest increment that could be differentiated on the calipers: 0.001 in. Similarly, this is the same error for the micrometer.

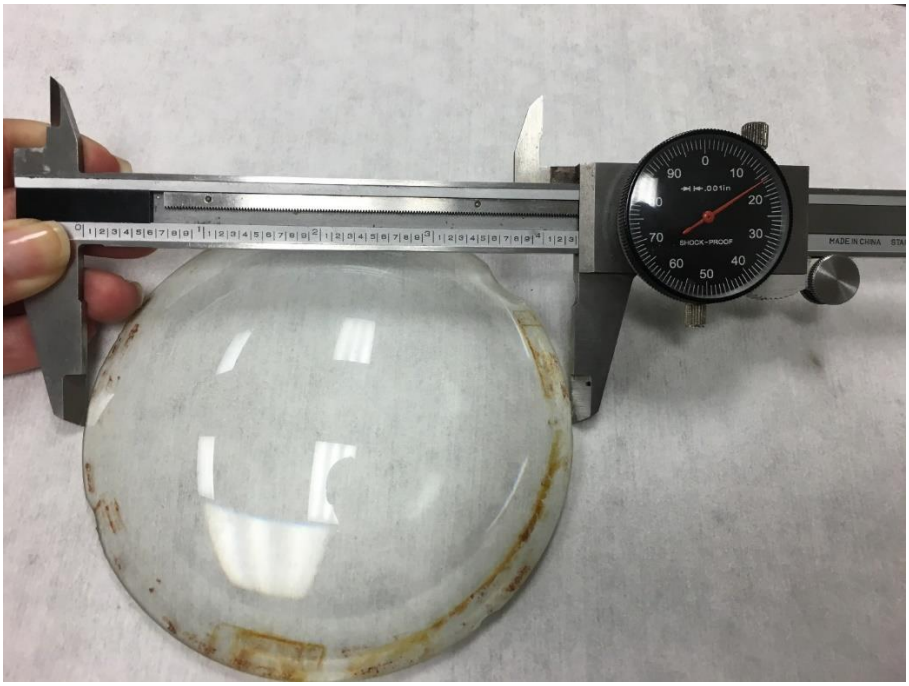

Figure 11: Thickness Measurement of a Lens in the Lab

3.1.2 Finding the Thickness of a Lens using a Micrometer

To measure the thickness of the lens a stand was constructed for the micrometer that could measure the displacement from the highest point on the convex surface, to the lowest point on the flat side of the lens. To do this the micrometer was suspended and set to its lowest setting. The height of the micrometer was adjusted so that the lens could barely slide beneath it at the highest point of the convex surface. Note that this method has a risk of scratching the optical surface and was only used here because the lens is uncoated and already heavily damaged. The lens was removed, the micrometer was rotated, which extended the spindle until it reached the surface which the lens previously rested on. The difference between these values (1.034 ± 0.001 in – 0.022 ± 0.001 in) generates the thickness of the lens t = 1.012 ± 0.0014 in as shown in the figure below:

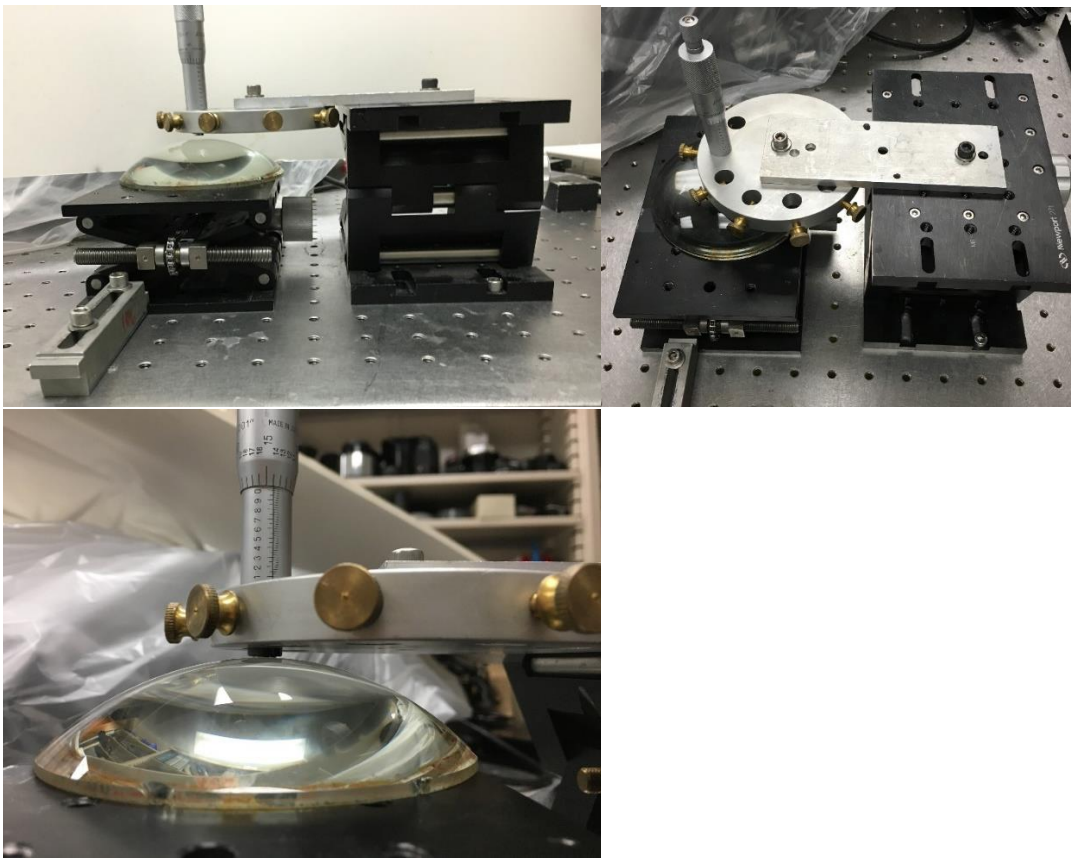

Figure 12: Side view of Micrometer setup for thickness measurement (top-left), Top view (top-right), and closeup (bottom-left).

3.1.3 Finding the Radius of Curvature of a Lens using a Spherometer

The radius of curvature can be calculated using the following relation in Figure 13 and equation 8:

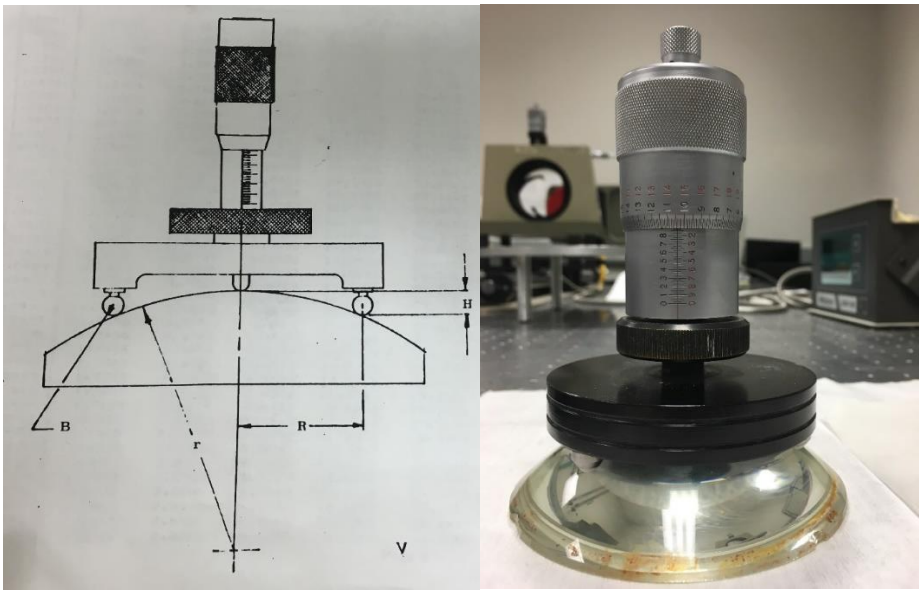

Figure 13: Radius of Curvature Measurement Using Spherometer (Strasbaugh, 1964).

$$r = \frac{R^2}{2H} + \frac{H}{2} \pm B \tag{8}$$

Where r = Radius of Curvature, B = radius of Contact Ball, H = Sagitta, R = Radial distance from the contact point to the central axis of the contact balls. For this case, R = 1.5 inches and B = 0.23 ± 0.005 inches. Here, R does not have an uncertainty because it is unknown, but assumed to be much less than any other contributing error. Using the spherometer the sag was measured to be H = 0.3824 in ± 0.0001 inches. Thus we get the final result below for radius of curvature:

$$r = \frac{1.5^2}{2(0.3824)} + \frac{(0.3824)}{2} - 0.23 = \ 2.90 \ \pm 0.005 \ inches \tag{9}$$

This value of the radius of curvature will be compared later with the value found interferometrically with the null configuration.

3.2 Flat surfaces

For the null testing configuration of the flat, the flat surface from the plano-convex lens 1 was used along with a flat reference surface configured with a Fizeau phase shifting interferometer (Wyko 6000). The goal of the setup is to have rays aligned with the optical axis retro-reflecting off of the flat UUT-surface. Lens 1 was not very good quality and had several chips on the edge of the surface. The resulting interferogram of the flat, therefore, is not the pristine interferogram that would be predicted of a flat surface using this null configuration (seen in Figure 15).

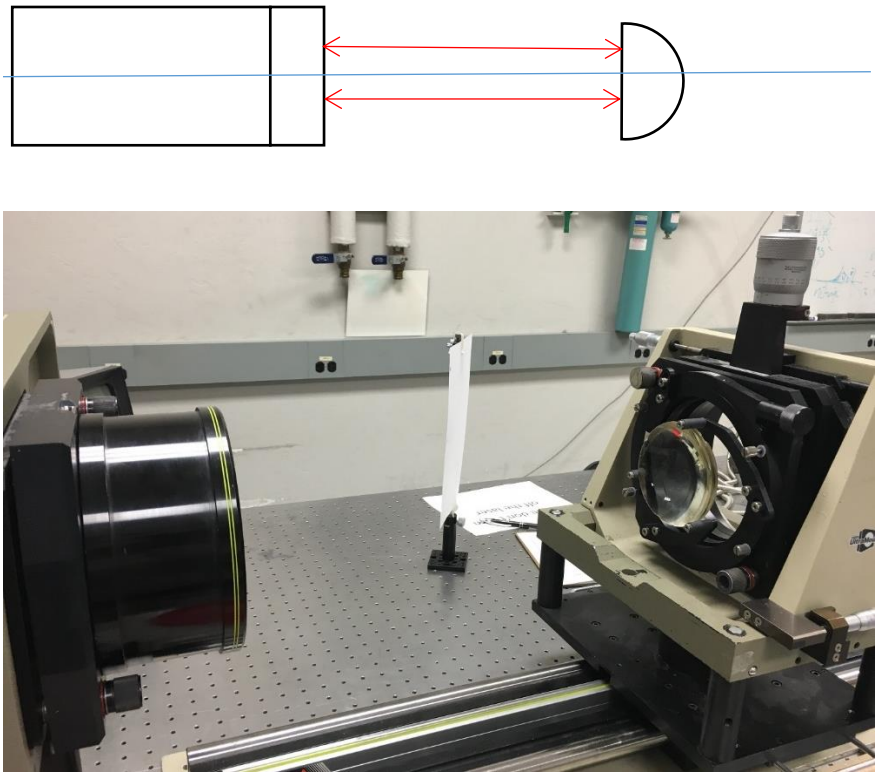

Figure 14: Ray-trace of measuring flat surface (top) and laboratory setup (bottom).

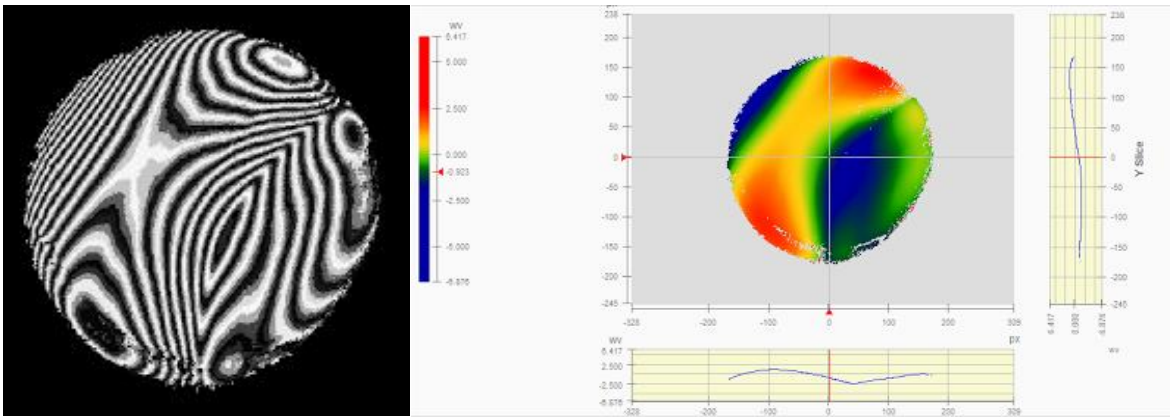

Figure 15: Interferogram from flat "null" test (left), and resulting surface figure contour plot (right).

3.3 Spherical surfaces

Null configurations of spherical surfaces are a little more complicated than those for plano-surfaces, but there is the tradeoff that they provide more information. With a plano-convex lens we can interferometrically determine the index of refraction and radius of curvature in addition to the surface figure that can be calculated using phase shifting methods. With the methods outlined below, our accuracy is only limited by the measurements of the lens's displacement as we find three different "null" positions for the lens and the interferometer.

In order to generate a null configuration, again it is desired for there to be no additional aberrations. This requires retro-reflection of the rays off the surface of interest, or an inversion of the original image. To create an inversion, focused rays from the top of the lens would follow the opposite path of focused rays from the bottom of the lens, and visa-versa as shown in Figure 16 and Figure 19.

3.3.1 Plano-Convex Configuration

To test the null configuration of the convex surface of a plano-convex lens, there are three positions of interest: the focus of the beam at the back convex surface (cats-eye configuration), the focus at the front flat surface, and the focus before the lens to generate a retroflection off the lens's back surface. These three configurations are demonstrated in Figure 16. Figure 16 also shows the interferogram at each of these three configurations.

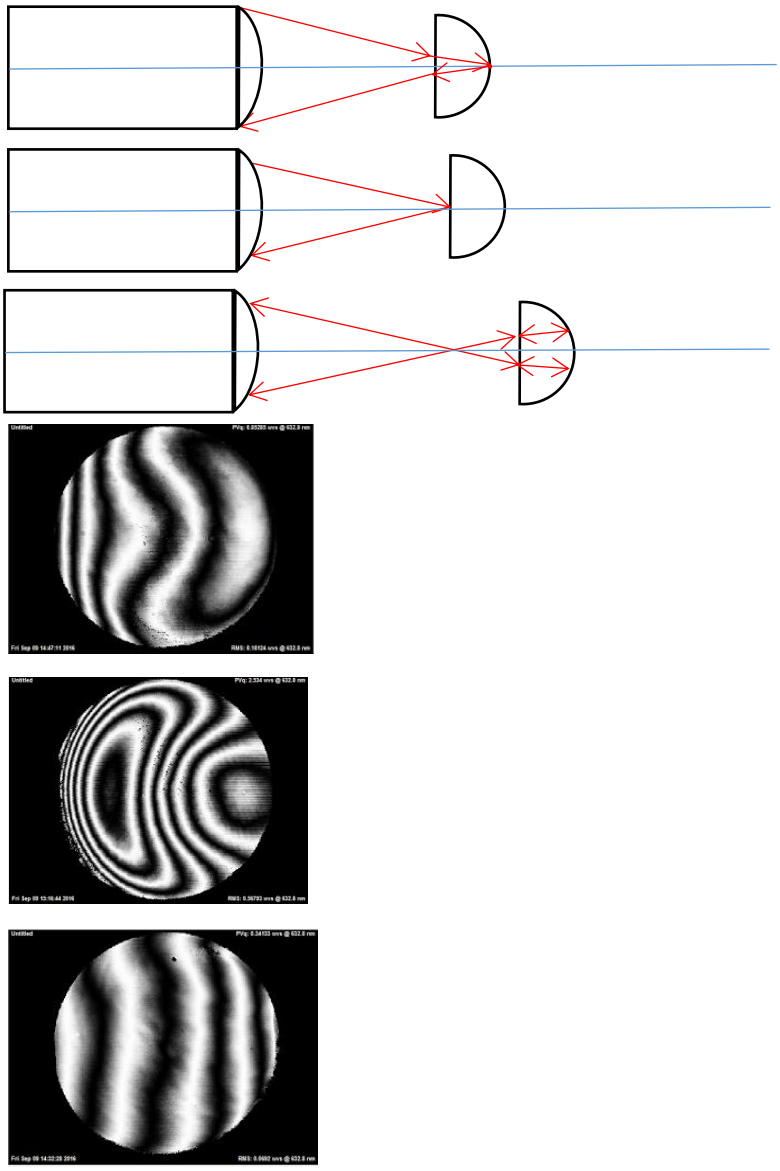

Figure 16: Catseye focus (top), front-focus (middle), and retro-reflection (bottom) – and their respective interferograms. Note: rays are not drawn to scale.

From the measurements taken, the index of refraction can be calculated by solving equation 10 for n (Greivenkamp, 2004).

$$d = \frac{n-1}{n}\, t \tag{10}$$

$$n = \frac{1}{1-\left(\frac{d}{t}\right)} \tag{11}$$

Where *d* is the displacement of the beam's focal point due to the glass's index of refraction *n*.

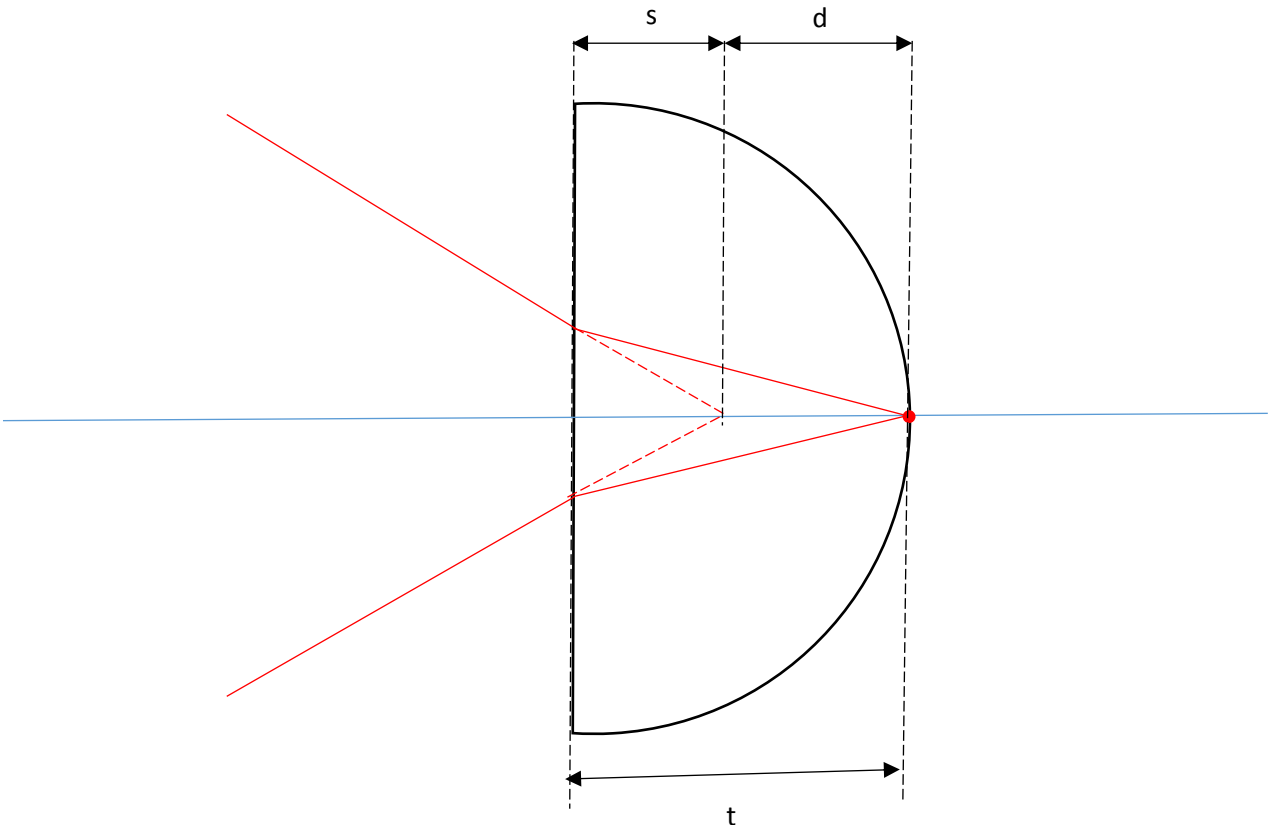

Figure 17: Null-Configuration Shifts and Reduced Thcikness to Find Index of Refraction

In Figure 17, *s* is the distance the lens must be translated to go from catseye to front-focus (it is the distance from the front-surface to where the light would focus if the lens material was air). *t* is the thickness of the lens calculated in section 3.1.2. Below are the measurements with the final results:

$$\begin{aligned} t &= 1.012 \pm 0.0014\ in \\ s &= 0.678 \pm 0.001\ in \\ d &= 0.337 \pm 0.001\ in \\ n &= 1.499 \pm 0.005 \end{aligned} \tag{12}$$

The uncertainty in the index was calculated via Section 7.1. Then, a Monte Carlo was performed in Section 7.2 to find the number of measurements that should be performed to ensure this uncertainty is one standard deviation above and below the mean when the index is measured over multiple trials.

A model of this system was created with the assistance of Dr. Sasian in Zemax as shown in the following figure. This model confirmed the index of refraction, n = 1.49 by replicating the f/# of the interferometer, the thickness of the lens I measured, and the catseye focus configuration from Figure 16. The focus on the back surface was chosen to be the smallest spot-size.

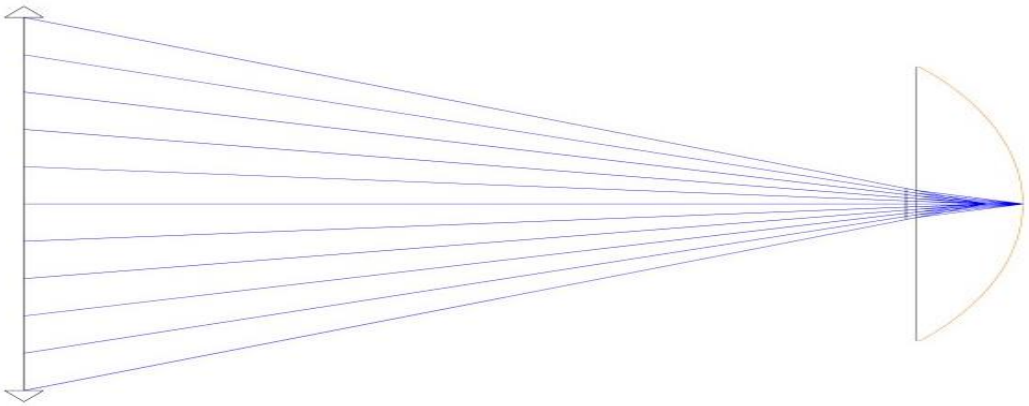

Figure 18: Zemax Model of Plano-Convex Catseye Null Configuration

3.3.2 Convex-Plano Configuration

To get additional practice in setting up null-configurations and aligning the interferometer, the tests from the above section were performed one more time, but in the convex-plano configuration. This had the added benefit of a simple interferometric way of confirming the radius of curvature found using the spherometer in section 3.1.3.

Similar to the plano-convex configuration, there are three setups: the retro-reflection configuration, focusing on the back of the lens, and focusing on the front of the lens (the cats-eye configuration). The difference is where these foci occur with the convex surface in front. These are demonstrated in Figure 19.

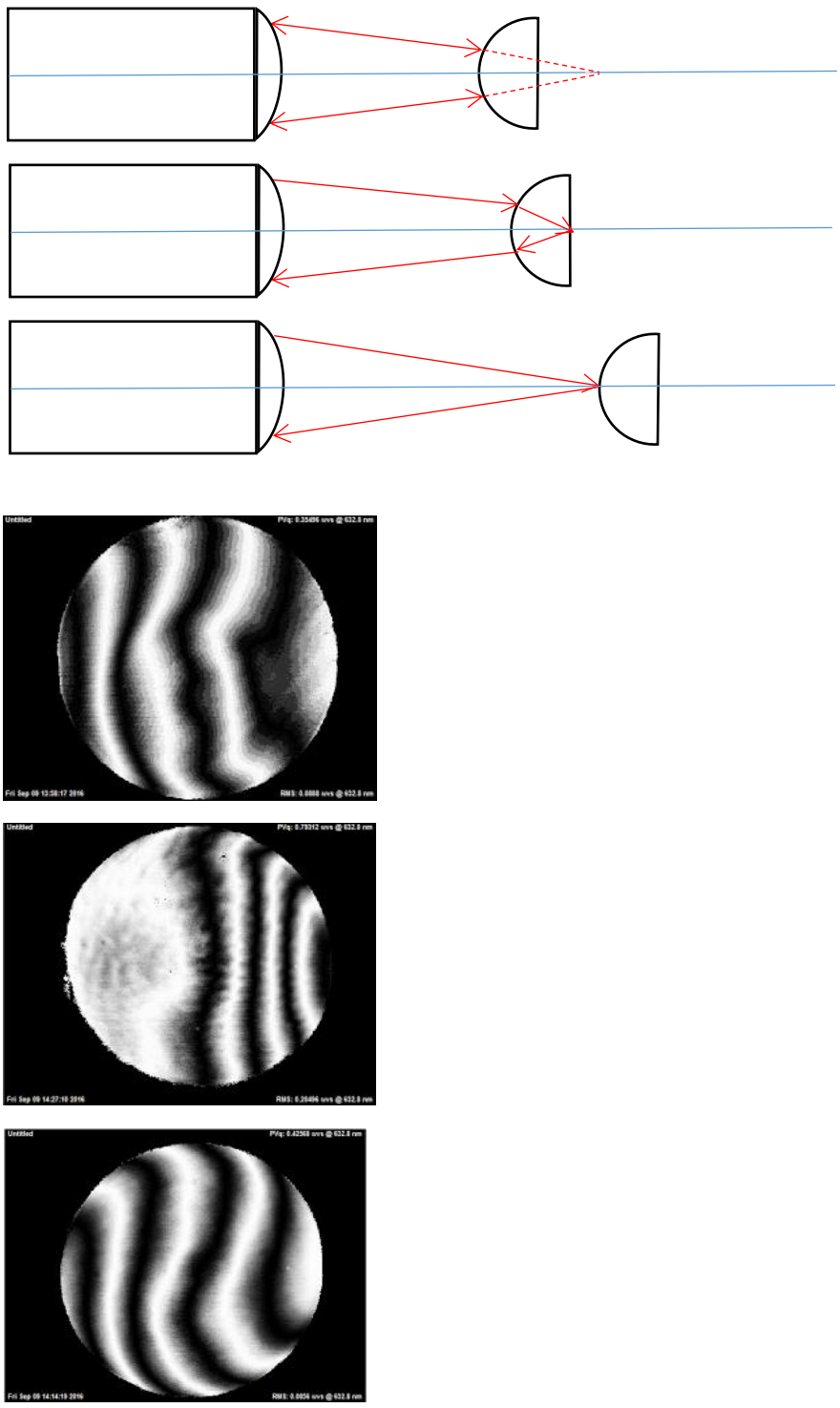

Figure 19: Retro-reflection (top), focus on back-flat (middle), and catseye focus (bottom); and corresponding interferograms. Note: rays are not drawn to scale.

From the figure above it is readily apparent that the radius of curvature can be found using these null-configurations. Since the retro-reflection configuration requires the rays to be perpendicular to the lens's surface, it is know that these rays would converge at the lens's center of curvature (had the lens not bent the light). The catseye configuration has these same rays focusing on the front-surface of the lens.

Therefore, the radius of curvature is the lens's shift between the retro-reflection and catseye configurations:

$$r = 2.953 \pm 0.001\ inches \tag{13}$$

The result above is very close to the radius of curvature found in section 17, with a percent-different of only 1.7% (when looking at the nominal values). Note that the uncertainty in the calculation above has only accounted for the uncertainty in the measurement scale of the rail. It was difficult to accurately account for the potential errors in measurement as the null-configurations were visually apparent over small ranges of motion.

3.4 Alignment of off-axis parabola

In the past, when a system called for an OAP, an entire parabola had to be ground and polished, with the section of interest being cut out – this a time consuming, and often prohibitively expensive task. OAP's have become more common in present years due to new, cheaper methods of fabrication via diamond turning and coordinate measuring machines that fabricate only the optic required. OAP's primary uses include collimating or focusing light – what makes these mirrors so special though, is that they do this along an angle offset from the original optical axis.

Due to the shape and off-axis nature of the OAP's, aligning these optics in a system is much more complicated than the usual on-axis optics. Luckily, there are steps taken to simplify the process based on knowing what aberrations will dominate the system (Parks, 1980). An attempt was made to follow the steps outlined in Parks' paper, *Alignment of Off-Axis Conic Mirrors*, but the OAP was in a fixed stand that did not allow certain, necessary, degrees of freedom (see Figure 23).

While Parks' paper has a rigorous mathematical derivation of the dominating aberrations within an OAP, a figure of the contour plots for a parabolic mirror make the aberrations much more apparent:

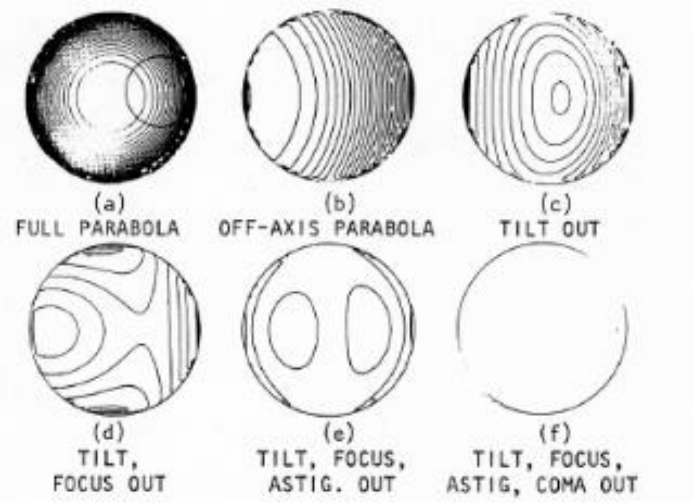

Figure 20: Contour plots of Off-Axis Parabolla with Aberrations iteritively removed (Parks, 1980)

Figure 20 shows the contour plots of a parabolic reflector, and these plots can be thought of as interferograms. Once the section of interest for the OAP (image b) is taken, it is seen that it heavily resembles a tilted optic. With the tilt removed, the telltale signs of astigmatism and a large amount of

defocus are seen, as there are a large number of rings with an elliptical shape (c). With defocus removed in (d) the rings now disappear and an asymmetric saddle appears, similar to the 50% astigmatism and 50% coma image from Figure 10 (except with more astigmatism). Image (e) shows that only coma remains once astigmatism is removed, and finally the interferogram is clear once the coma is removed (Parks, 1980). Parks' mathematical derivation shows that in fact the interferogram still contains spherical aberrations, but it is at least 8 times smaller than the coma's weight.

In practice, to begin aligning the OAP, a screen was placed where the light reflected off the surface to determine a location of best-focus by finding the smallest spot. Note, this spot is reflected only slightly off-axis, as it was right next to the interferometer's output, as shown in Figure 21.

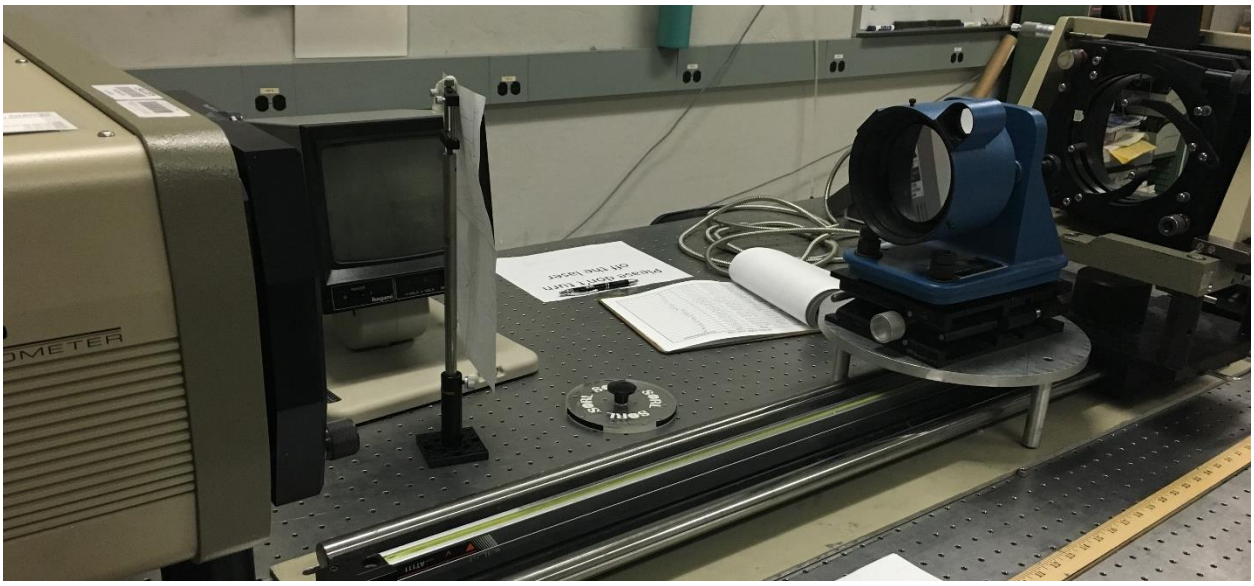

Figure 21: Test Setup for Alignment of Off-Axis Parabola

With this current setup, the sagittal and tangential astigmatic lines were generated (examples of astigmatic lines are shown in Figure 22), but the screen required a translation of roughly 7mm between the two. To minimize this distance, two parameters were adjusted: tilting the blue-mount left and right (yaw), and tilting the blue-mount up and down (pitch). This was a tedious iterative process as one parameter would be slightly changed and then the translation in the screen was measured between tangential and sagittal lines. This was complicated by the fact that the OAP was at a fixed clocked position within the blue mount (Figure 23), so the plane of incidence for the reflected light was not the plane of the table. Thus, a shift of the dot along just one axis required careful adjustments of both degrees of freedom.

Figure 22: Example Astigmatic Lines. Tangential focus (left), Medial Focus (center), Sagital Focus (right) (Parks, 1980).

Although the distance was minimized between sagittal and tangential focus, the reflection off the OAP was not parallel with the table. This proved to be a prohibitive issue because the final step in alignment is to place a flat or ball in the beam's path to reflect the light back into the interferometer, thus creating an interferogram. It was decided to stop at this point, since aligning a reflective surface to this vertically angled beam complicated the system beyond the learning benefit this exercise presented. Since this project was not seen to completion, instead the testing in section 3 for the majority of this report was performed.

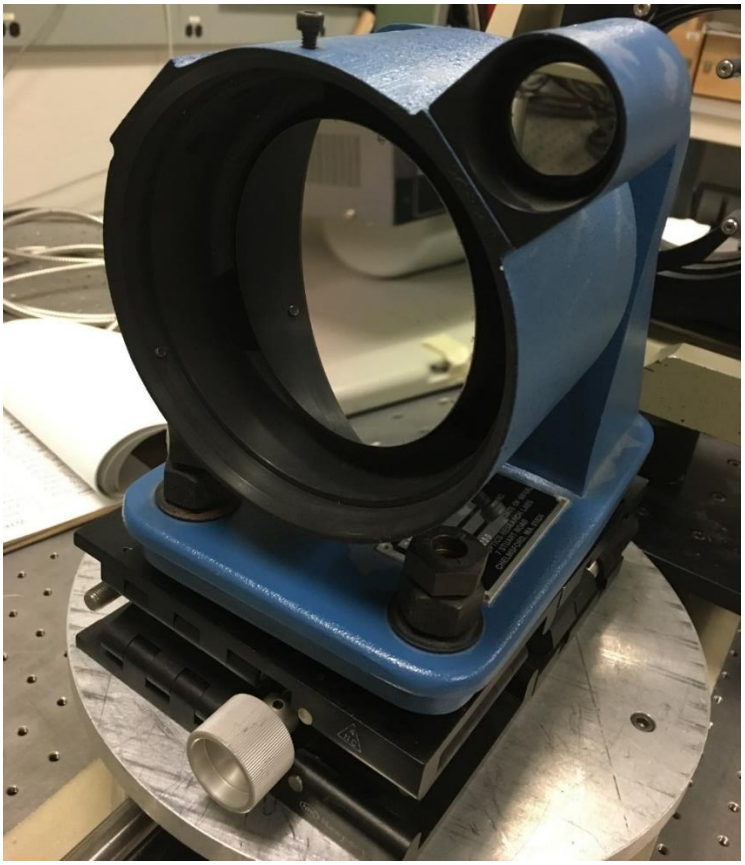

Figure 23: Closeup of Off-Axis Parabola, showing mirror enclosed in blue mount

4 Conclusion

In this report two types of interferometers were discussed: Newton and Fizeau. The Newton interferometer provided a simple architecture to describe the fringe patterns that emerge from observing light reflecting off two surfaces. This type of interferometer can be used in optics shops for either quick estimates of surface figure, or more in-depth calculations by relating the distance between fringes to the variations in the air gap between a reference and the UUT (Equation 4). A Fizeau interferometer uses the same principles, but its setup is more amenable to larger air gaps and it can yield higher accuracy by introducing phase shifting. Phase shifting algorithms' primary purpose is to gain data with every pixel, while averaging out the noise inherent in the system.

The Fizeau interferometer was the focus of the experimental aspect of this report since a Wyko 6000 Fizeau phase shifting interferometer was used to conduct the majority of the measurements. Using this

Fizeau interferometer, several null configurations were tested for a flat and plano-convex lens. The purpose of testing the different null positions was to gain experience using a professional interferometer, and aligning the optics to this interferometer. Even though a basic visual determination was used to decide the null positions, a nearly equivalent result was measured for the radius of curvature between the interferometric method ($r = 2.953 \pm 0.001\ inches$) and the use of a spherometer ($r = 2.90 \pm 0.005\ inches$) resulting in a percent-difference of 1.7%. The index of this same lens was also found interferometrically to be $n = 1.499 \pm 0.005$.

Additionally, aberrations of optics were discussed in the context of completed lenses and mirrors under fabrication. One often-used technique is to add tilt to an interferogram, as deviations from the straight fringes are more easily translated into other aberrations. An important topic of study is not just individual aberrations, but combinations of them, since it is unlikely an optic will contain just coma or just astigmatism. By being able to translate an interferogram's fringe patterns, a qualitative estimate of the dominant aberrations can be determined.

For the OAP, despite only doing the rough alignment, the importance of a good alignment plan and patience was learned. It also provided an experience to better understand astigmatism as the primary aberration of this system. The sagittal and tangential astigmatic lines were observed and minimized through many iterative steps to complete the rough alignment of the OAP.

The knowledge gained during the course of this report – from performing the testing, to transcribing the theory– has provided practical optical test engineering experience, which was the driving motivator for pursuing a masters in optical sciences.

5 Acknowledgements

A special thanks to Dr. Jose Sasian for his mentorship and large contributions to helping me understand and perform the testing in this report. Also to my other panel members Dr. Jim Schwiegerling and Dr. Yuzuru Takashima. Finally, to Chris Janich for his never-ending support in all things.

6 References

DeGroot, Peter. (1997). 101-Frame Algorithm for Phase Shifting Interferometry. *Optical Inspection and Measurements II, 283*.

Frieden, B. (2001). *Probability, Statistical Optics, and Data Testing.* New York: Springer.

Green, M. (n.d.). *WebMathematica and LiveGraphics3D*. Retrieved from Aberrations, Table, Plots, and Equations: http://wyant.optics.arizona.edu/webMathematica/myprograms/OPDPlotsMargy/AberrationsTablePlotsEquations.pdf

Greivenkamp, J. E. (2004). *Field Guide to Geometrical Optics.* Bellingham, Washington: SPIE.

Hariharan, P. (1999). Phase Shifting Interferometry: Minimization of Systematic Errors. *Optical Engineering*, 39(4):967-969 .

Malacara, M. V. (2007). Newton, Fizeau, and Haidinger Interferometers. In D. Malacara, *Optical Shop Testing.* Hoboken, New Jersey: John Wiley & Sons Inc.

Murty, M. V. (1978). Newton Fizeau and Hainger Interferometers. In D. Malacara, *Optical Shop Testing* (pp. 1-34). Tonantzintla, Pue. Mexico: Instituto Nacional de Astrofisica.

Parks, R. E. (1980). Alignment of Off-Axis Conic Mirrors. *College of Optical Sciences, University of Arizona*.

Schwiegerling, J. (2014). *Optical Specification, Fabrication, and Testing.* Bellingham, Washington: SPIE.

Strasbaugh, R. H. (1964). *Spherometers: Radius of Curvature Tables.* San Luis Obispo, CA.

7 Appendix

7.1 Error Analysis

Addition and Subtraction

Given two values which have uncertainties, $a \pm \delta a$, and $b \pm \delta b$, finding the error when adding (or subtracting) these two values requires adding their error in quadrature:

If $Q = a + b$, then $\delta Q = \sqrt{(\delta a)^2 + (\delta b)^2}$

For example, in the case of the thickness measurement of lens 1, two measurements were taken and then subtracted:

t = 1.034 in ± 0.001 – 0.022 in ± 0.001

$\delta t = \sqrt{(0.001)^2 + (0.001)^2}$ = 0.0014

Multiplication and Division

To find the error when multiplying (or dividing) two values, one would add the ratio of their error to their value in quadrature:

If $Q = a \times b$ then $\delta Q = \sqrt{\left(\frac{\delta a}{a}\right)^2 + \left(\frac{\delta b}{b}\right)^2}$

7.2 Monte Carlo Analysis and Central Limit Theorem

The Central Limit theorem states that the distribution of the sum of a random variable over numerous trials tends towards a normal distribution, given a large enough sample set. A rigorous mathematical proof of this theorem is found in section 4.25 of (Frieden, 2001). The variance (and thus standard deviation) of this sum is primarily dependent on the number of random variables summed per trial.

This theorem is applied to the index of refraction, calculated via equation 11. The index is a random variable dependent on two independent random variables: the lens thickness (*t*) and the distance the lens is displaced between null configurations (*d*). A Monte Carlo analysis was run to simulate *t* and *d* being measured *M* times, and the resultant index *n* being averaged to generate $\bar{n}$. This index was averaged over *N* trials and the distribution of $\bar{n}$ is indeed a normal distribution, as shown in Figure 24.

The results of this figure show that after 8 measurements of *t* and *d*, the resultant mean index of refraction has a 68% chance of being contained within the uncertainty calculated using the results of Section 3.3.1

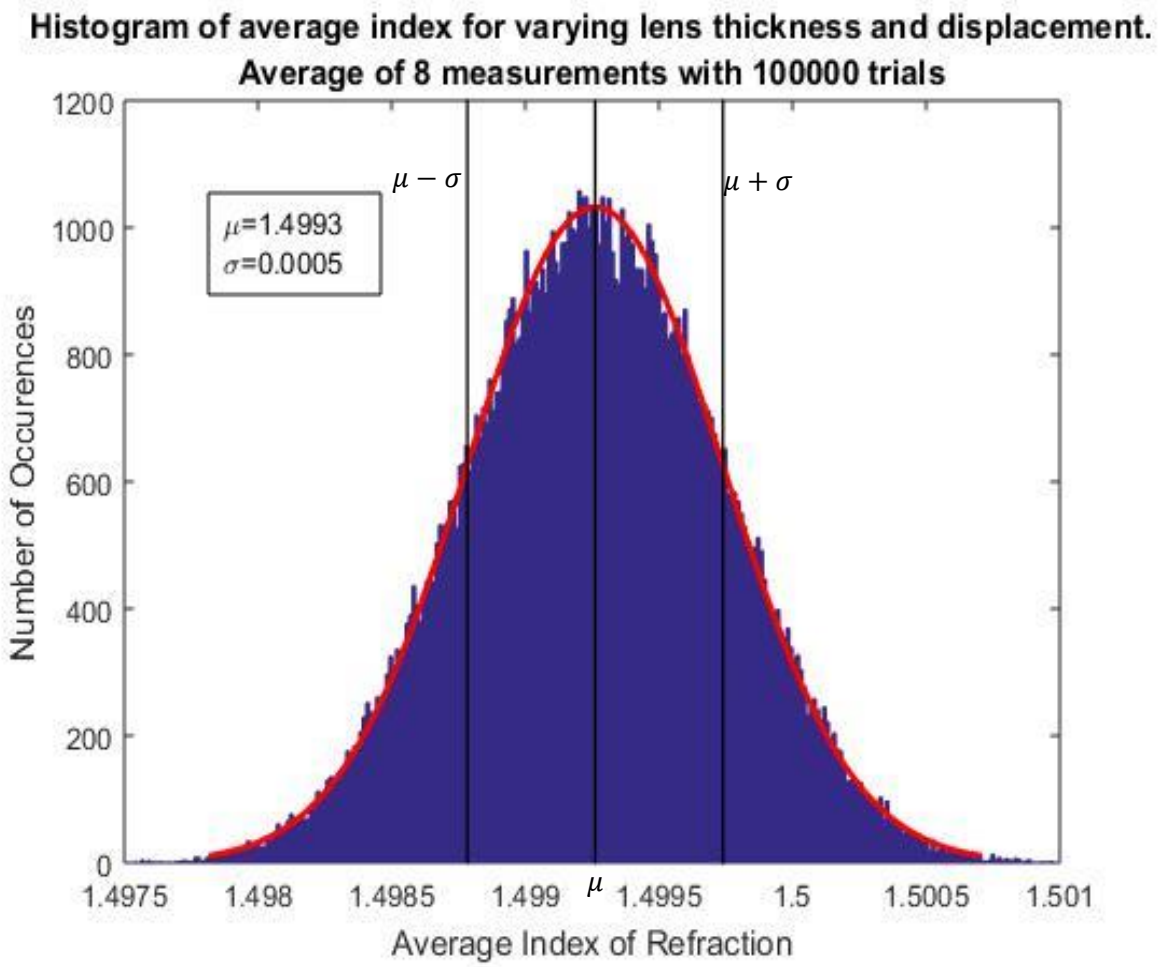

Figure 24: Monte Carlo Analysis of Index of Refraction